Available online at www.sciencedirect.com

ScienceDirect

journal homepage: www.elsevier.com/locate/he

ELSEVIER

Scheme of thermal compression of hydrogen (TCH) using MmNi$_{4.25}$Al$_{0.75}$ recovered with ethyl alcohol and handled under non protective atmospheres

CrossMark

S.A. Obregón [a,b,c], M.R. Esquivel [b,c,d,*]

[a] Instituto Balseiro, UNCu and CNEA, Av. Bustillo km 9.5, Bariloche R8402AGP, Argentina
[b] Consejo Nacional de Investigaciones Científicas y Técnicas (CONICET), Argentina
[c] C.R.U.B.-U.N.Co, Quintral 1250, R8400FRF Bariloche, Río Negro, Argentina
[d] Centro Atómico Bariloche, Comisión Nacional de Energía Atómica (CNEA), Argentina

ARTICLE INFO

ABSTRACT

A MmNi$_{4.25}$Al$_{0.75}$ intermetallic was obtained by low energy mechanical alloying and low temperature heating at 600 °C for 24 h under Ar. The intermetallic was recovered from milling chamber using ethyl alcohol, dried, stored and handled under air at room conditions. Structure was characterized by XRD. A maximum stability temperature of 160 °C was obtained from non-isothermal DSC measurement under air. The kinetics of oxidation at 200 °C was analyzed. A maximum reaction degree ($\alpha = 0.1$) was obtained after 2500 s of treatment. The hydrogen sorption properties of samples were studied by volumetric measurements. Hydrogen maximum mass percent capacity (mass %) was reached in less than 300 s. The thermodynamic sorption properties were measured. Values of $\Delta H_f = -29 \pm 2$ kJ mol^{-1} and $\Delta S_f = 197 \pm 10$ J mol^{-1} K^{-1} were obtained for absorption process and $\Delta H_d = 28 \pm 2$ kJ mol^{-1} and $\Delta S_d = 189 + 10$ J mol^{-1} K^{-1} were obtained for desorption process. From these results, a one-stage of thermal compression of hydrogen is proposed with a standard compression ratio (R_c) of 5.71 in the 25–80 °C range.

Introduction

The synthesis and experimental handling of highly reactive hydride-forming materials is favored by the current advanced research and design of glove boxes and diverse devices developed to avoid contact of samples with laboratory atmospheres. Under these controlled atmospheres, either water and oxygen contents are lower than a 0.01 ppm. This current technological condition allows the synthesis of new structures related to these compounds and the discovery of new thermodynamic hydrogen sorption properties [1–3]. Despite these necessary and successful findings, the engineering of the scaling up from laboratory to larger prototypes should avoid inert conditions to diminish the investment in hardware and expenses related to the handling of large amounts of hydride-forming materials. For engineering applications, this situation makes the research work to face the unavoidable
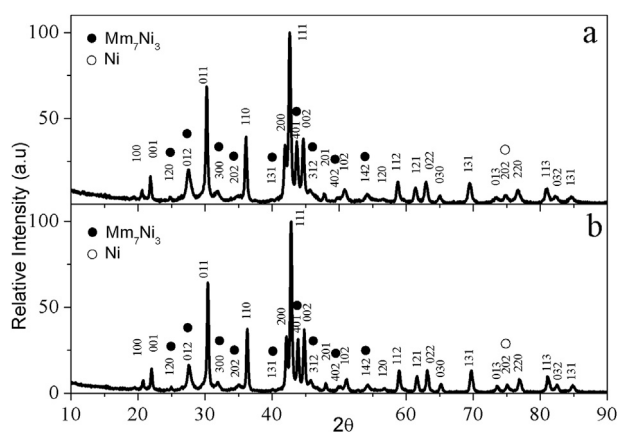
Fig. 1 − a) Diffractogram of as-milled + annealed sample. b) Diffractogram of the sample after hydrogen absorption−desorption treatment.

option of study both the structural and hydrogen sorption properties of materials handled under non inert atmospheres: mostly air at room conditions. Then, the properties of hydride-forming materials are analyzed to the light of a more realistic handling: the resistance of these materials to contamination/deterioration after storing under atmospheric conditions and before the use in diverse applications of the hydrogen technology [4]. Keeping that objective in mind, a $MmNi_{4.25}Al_{0.75}$ intermetallic was obtained by mechanical alloying-low temperature heating treatment using a method reported previously [5,6]. Remaining sample was recovered from milling chamber with ethyl alcohol, dried and stored at room conditions. After that, the hydrogen sorption properties were studied. The results are used in the design of a one-stage thermal hydrogen compression scheme. In this type of device, no moving parts are used [4]. Therefore, hazards due to hydrogen leaks are decreased. Then, security in laboratory/commercial buildings is improved. These objectives aimed the elaboration of this work.

Experimental

Ni powder (Sigma/Aldrich, 99.99%, −100 Mesh), chunks of Mm ($La_{0.25}Ce_{0.52}Nd_{0.17}Pr_{0.06}$, Reacton, 99.6%) and Al (Aldrich, 99.99%, Flakes 100 μm) were set with stainless steel balls in a stainless steel chamber under Ar atmosphere to obtain an intermetallic of nominal composition $MmNi_4Al$. The mixture

was mechanically alloyed in an Uni-Ball-Mill II apparatus (Australian Scientific Instruments). A ball/sample mass ratio of 11.2 was selected. Encapsulated samples were annealed in a laboratory oven (INDEF model 331). Room temperature X-ray diffraction (XRD) was achieved on a Phillips PW 1710/01 instrument and PANalytical Empyrean with Cu K_{α} Radiation (graphite mono-chromator). Strain (s) and crystallite size (D) values were estimated from diffraction peaks by considering Gauss and a Lorentz contribution, respectively [7]. Chemical composition was verified by Energy Dispersive Spectroscopy (EDS) analysis using a device associated to a SEM 515 (Philips) microscope. Thermal analysis was done by using Differential Scanning Calorimetry (DSC 2970, TA Instruments). Measures were done under air at 2 °C min^{-1} and isothermal measurements were done at 200 °C. The hydrogen sorption properties were measured in a Sievert's type device. Pressure-composition-isotherms (PCI) were done between 25 and 80 °C. The hydriding kinetic behavior was analyzed at 25 °C and 80 °C.

Discussion and results

Structure characteristics, thermal stability and kinetics of the oxidation in air

Fig. 1(a) shows the diffractogram of the sample obtained by mechanical alloying followed by thermal treatment at 600 °C for 24 h in Ar. Three phases were identified. An hydride-forming AB_5 and two extra phases: Mm_7Ni_3 and Ni. The structural parameters and sample mass value of these phases is presented in Table 1. The composition of the hydride-forming AB_5 was obtained from a crystallographic model developed ad-hoc [8]. The model evaluates the change of the structural parameters associated to the replacement of Ni by Al in Wyckoff positions 2c and 3g [8]. The composition values estimated using this method are more accurate than EDS measurements because the model considers the changes on the structural parameters of the AB_5 while EDS measurements analyzes the global sample including the other two phases. A comparison between nominal composition, EDS measurement and composition obtained using the crystallographic model is presented in Table 3. The diffractogram of Fig. 1 shows an appropriate peak to background ratio related to a mild crystallite size distribution. The microstructural values are summarized in Table 3. The crystalline characteristics are less developed than samples obtained by high temperature methods [4] (see Table 2).

Table 1 − Structural data of samples. Mm is the nominal composition $La_{0.25}Ce_{0.52}Nd_{0.17}Pr_{0.06}$. Mass sample % was obtained using the single peak method.

Sample treatment	Phase	Space group	a [Å] ± 0.002	c [Å] ± 0.002	α	γ	Mass % ±1%
Milled 120 h and annealed 600 °C 24 h	$MmNi_{4.25}Al_{0.75}$	$P6/mmm$	4.959	4.048	90	120	65%
	Mm_7Ni_3	$P6_3mc$	10.020	3.389	90	120	34%
	Ni	$Fm3m$	3.525	—	90	—	∼1%
Cycled with hydrogen	$MmNi_{4.25}Al_{0.75}$	$P6/mmm$	4.959	4.048	90	120	63%
	Mm_7Ni_3	$P6_3mc$	10.020	3.389	90	120	35%
	Ni	$Fm3m$	3.525	—	90	—	2%

Table 2 – Microstructural properties of the MmNi$_{4.25}$Al$_{0.75}$ for representative hkl values.

Sample treatment	h k l	D (Å) ± 10 Å	s (%) ± 0.05%
Milled and annealed	101	450	0.2
(Fig. 1(a))	110	430	0.2
After cycling in hydrogen	101	360	0.3
(Fig. 1(b))	110	360	0.2

Fig. 1(b) shows the sample after hydriding cycles. The structure remains stable and no extra phases appear. No sample mass % increase of the other phases occurs as deduced from the values presented in Table 1. The general effect of the hydriding cycles is a decrement in crystallite size and increase in strain as typically reported for these compounds [9].
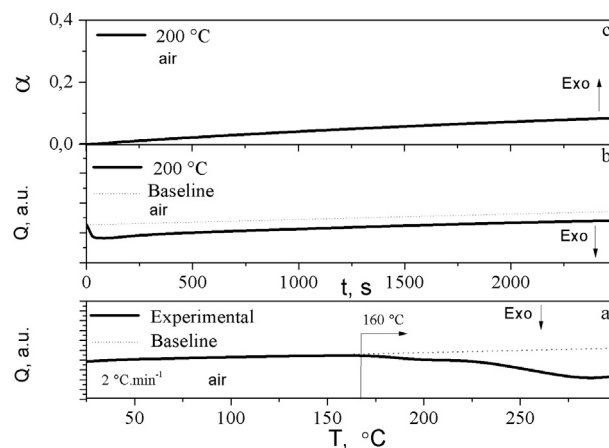
Fig. 2(a) shows the non-isothermal DSC measurement of the sample under stagnant air at a heating rate of 2 °C min^{-1}. The experimental data departs from the baseline near 160 °C. Then, this temperature is considered as the starting destabilization of the intermetallic (IM). As temperature increases, the heat evolved increases and data departs from the baseline. The thermal decomposition of the IM is a complex process that includes the endothermic decomposition of the IM followed by the exothermic oxidation of the individual constituents of the IM [10]. This temperature value is a relevant result because this type of IM is used in open-cycles of thermal compression. This application normally operates between room temperature and 90 °C [4,11,12]. Then, this temperature value is an adequate security margin (T range > 60 °C) which ensures that IM can not be decomposed if accidentally contacts air under operating conditions. An isothermal DSC measurement is done to estimate the kinetics of the oxidation. It is shown in Fig. 2(b). As observed, the exothermal evolution of the sample is slow and a maximum $\alpha = 0.1$ is reached at 2500 s. This low reactivity towards the thermal decomposition is a relevant result because if produced, contact of the sample with air at operative conditions either do not react (T < 160 °C) or it has a slow kinetics of reaction (T < 200 °C).

The hydrogen sorption properties

Sample was recovered from chamber by successive washing steps with ethyl alcohol. The alcohol of the intermetallic-alcohol suspension was led to evaporate at room conditions. After that, dried intermetallic remaining as powder in the bottom of the vessel was stored also at room conditions. Previous to activation, sample was heated at 200 °C for 1 h to vacuum to desorb the adsorbed species and remaining alcohol. After that, sample was activated for near 30 cycles of hydrogen absorption and desorption at room temperature. To analyze

Table 3 – Composition of the AB$_5$ phase calculated using different methods and techniques.

Measurement technique/ method	Composition obtained/ calculated
Nominal	MmNi$_4$Al
EDS	MmNi$_{3.6}$Al$_{1.4}$
Crystallographic model	MmNi$_{4.25}$Al$_{0.75}$


Fig. 2 – DSC measurements. a) Non-isothermal. b) Isothermal. Heat evolution. c) Isothermal. Reaction degree (α) evolution.

the equilibrium hydrogen sorption properties, the corresponding pressure-composition-temperature (PCI) curves were measured in the 25–80 °C temperature range. Some of the PCI's are shown in Fig. 3. Although the theoretical H% m/m value for typical AB$_5$'s is not reached [13], it has to be kept in mind that these samples were recovered from milling chamber walls, removed with alcohol, dried and stored at room conditions. Despite these unfavorable conditions, the maximum H% m/m reach a value as high as 0.8% at 25 °C. The PCT curves are also relatively flat as compared with samples obtained from high temperature methods and also treated in air [4].

Application to thermal compression of hydrogen

The scheme of thermal compression of hydrogen is presented in Figs. 3 and 4. Point I stands for the conditions of fresh
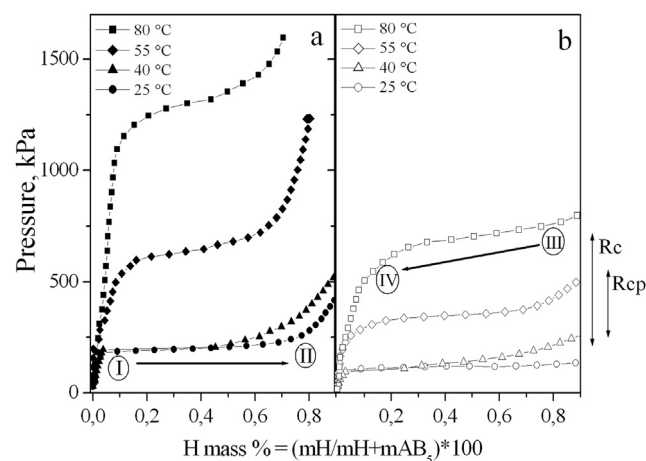
Fig. 3 – a) Absorption PCI curves (full dots). b) Desorption PCI curves (hollow dots). I–II–III–IV representative points of the complete TCH cycle. R$_c$ is the standard compression ratio (Ratio between middle plateau pressures). R$_{cp}$ is the practical compression ratio. (Ratio of the maximum absorption pressure to the minimum desorption pressure).
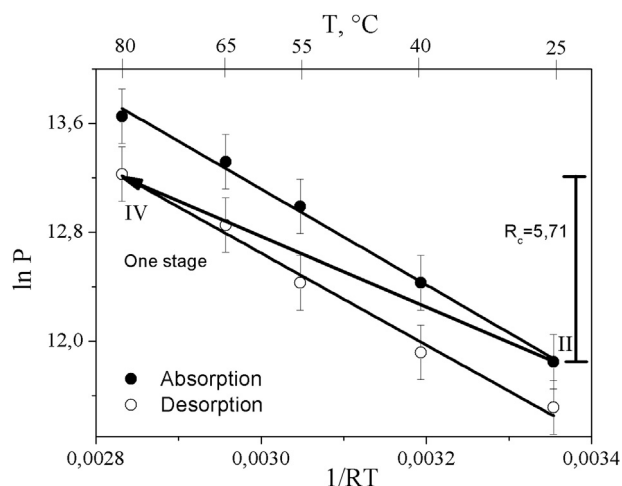
Fig. 4 — The Van't Hoff diagram. Points II and IV stand for the points of completion of supply of hydrogen and final exit of the compressed fluid. The R_c value obtained is 5.71.

hydrogen supply ($T = 25$ °C, $p = 125 \pm 5$ kPa). The hydride is formed according to the PCI at this temperature and system reaches point II going through a thermodynamic path described by this PCI. At point II, the system is isolated. Hydrogen supply is cut and the system is heated to 80 °C. The system is now at point III. Removal of hydrogen is done and the system goes to the path described by PCI at 80 °C reaching point IV. The compression stage can be clearly observed in the Van't Hoff diagram of Fig. 4. It is obtained using the equilibrium pressure values of Fig. 3. Full circle points stand for absorption values. Hollow circle points stand for desorption values. For absorption, the thermodynamic values obtained are $\Delta H_f = -29 \pm 2$ kJ mol^{-1} and $\Delta S_f = 197 \pm 10$ J mol^{-1} K^{-1}, respectively. For desorption, these values are $\Delta H_d = 28 \pm 2$ kJ mol^{-1} and $\Delta S_d = 189 + 10$ J mol^{-1} K^{-1}. Thermodynamic sorption values are similar to those of AB$_5$'s with similar composition [14]. The one-stage compression is schematized in this Figure. Point II represents the thermodynamic conditions described in the absorption isotherm at 25 °C and 125 ± 5 kPa. After hydride formation, the system is heated at 80 °C. According to the isotherm at this temperature, hydrogen is evacuated at 750 ± 5 kPa. Dehydrided IM is obtained. Then, system is cooled to 25 °C. At this condition, the system is ready to start a new hydrogen thermal compression cycle. As a result hydrogen was compressed in a $R_c = (750 \text{ kPa}/125 \text{ kPa}) = 5.71$ standard compression ratio. The practical compression ratio (R_{cp}) is calculated taking the higher absorption pressure at 25 °C and lower desorption pressure at 80 °C. The value obtained is $R_{cp} = (600 \text{ kPa}/225 \text{ kPa}) = 2.63$. Since the hydrogen is stored as a hydride, a solid matrix, the hazards due to hydrogen leaks is decreased. This situation normally arises in devices with moving parts. This AB$_5$-H$_2$ systems has an extra advantage. It is oriented to stationary applications such as the equivalent to fossil fuel gas stations. Therefore, the ratio sample mass/hydrogen volume is not a restriction. This means that small hydrogen-at laboratory-scale compressors can perfectly fit for supply of compressed hydrogen. The device is especially useful in tandem devices such as hydrogen compression systems — hydrogen electrolysers [15].

The kinetics of the sample absorption at 25 °C and desorption at 80 °C are presented in Fig. 5. These conditions were selected because the dynamics of the compression system are determined by these hydriding processes. These kinetics are the ones of path I to II and III to IV shown in Fig. 3. Hydriding at 25 °C is done in almost three stages. The first one is faster (t ~ 30 s) and reach $\alpha \sim 0.72$. The second and third are slower and the maximum α is reached in approximately 300 s. This indicates that the kinetic of hydriding/dehydriding process is faster than the kinetics of oxidation as observed in Fig. 2(c). This result is relevant because if the hydrogen fresh supply is contaminated with oxygen, the hydride formation should be faster at 25 °C since the IM do not react with oxygen at this temperature. The risk present in this case is the exothermal hydrogen/oxygen reaction in this closed system.

Dehydriding at 80 °C is also fast. The first stage reaches α ~0.72 for t ~30 s. The second and third stage are slower than the first. The maximum α is reached at ~300 s. The desorption leads to point IV. The hazard is present if oxygen enters accidentally to the system. At this temperature, the dehydriding process should not be slower than 350 s and the IM do not react with oxygen as observed in Fig. 2(b) and (c). Then, the low reactivity of the IM towards oxygen and the fast hydriding/dehydriding processes decrease de possibility of hazards in the TCH scheme. The possibility of application to industrial level is favored because hydrogen absorption and desorption rates are faster than pumping of hydrogen either for vacuum or filling for semi-industrial compression installations where alloys of similar composition were used [16]. A comparison between the energy consumption (kW h^{-1}) between this compressor and a conventional one was made. The comparison was based on the compression of a normal cubic meter of hydrogen. Energy balance in this compression system was done by considering the amount of water and corresponding energy consumption (heating and cooling devices and pumping systems) needed to maintain the hydrogen absorption temperature at 25 °C according to the isotherm of Fig. 3(a), to heat the system to 80 °C, to maintain the hydrogen desorption temperature at 80 °C according to the isotherm of Fig. 3(b) and to cool the system to
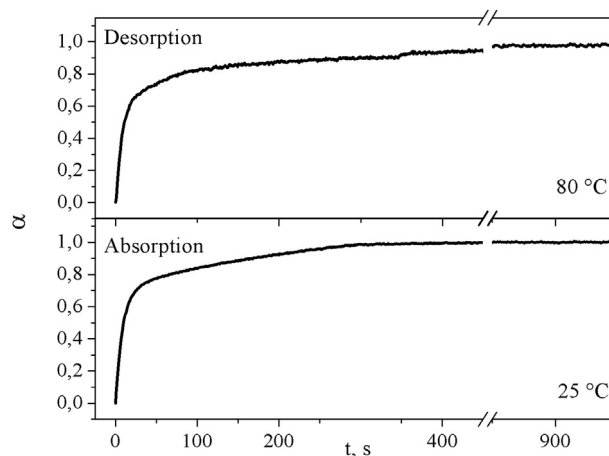
Fig. 5 — Kinetics of the processes of hydrogen absorption (25 °C) and desorption (80 °C). In these figures $\alpha = (\text{H mass }\%(t) - \text{H mass }\% (t_0))/(\text{H mass }\%(t_0))$. In this equation, t_0 is the starting measurement time.

25 °C in a similar fashion to metal hydride compressor estimations reported elsewhere [17]. The comparison with a conventional compressor was based on considering the efficiency and energy consumption needed to rise the pressure from 1 to 5 bar according to the specification of the compressor in a laboratory-scale. The values obtained are ~0.2 kWh and ~7.4 kWh for conventional compressor and metal hydride compressor, respectively. These values indicate that the operating conditions are more expensive than those of the conventional compressor. It is worth to note that calculations are done without optimizing mass/heat transfer in neither of these devices. Despite that current disadvantage, the security of the solid storage of hydrogen against hydrogen fluid leaks encourage the use of metal hydride thermal compressors.

Summary and conclusions

The road from the hydrogen economy to the hydrogen civilization [18,19] also involves the development of materials research focused in low cost of investment and expenses and low waste generation. This scope of research covers the synthesis and handling of large amounts of hydride-forming materials oriented to applications of the hydrogen technology. Then, the following results found in this paper contribute to achieve that final objective:

➢ The $MmNi_{4.25}Al_{0.75}$ can be recovered from milling devices by successive steps of washing with alcohol. The IM is stored and handled at room conditions.
➢ The structure resists heating under oxygen-content atmospheres up to $T > 160$ °C.
➢ The kinetics of the oxidation of the $MmNi_{4.25}Al_{0.75}$ in air is slow. In the case of hazard events, the IM can resist the decomposition/oxidation process.
➢ Despite the handling under non inert atmospheres, the hydriding properties are appropriate enough to develop a TCH scheme with a R_p of 5.71 and R_{cp} of 2.63.
➢ The hydriding/dehydriding kinetics are faster than the oxidation ones. It is a secure characteristic in events associated to desorption processes because hydride can be completely desorbed before the IM is decomposed by oxidation.

Acknowledgments

REFERENCES

[1] Sakintuna B, Lamari-Darkrim F, Hirschter M. Metal hydride materials for solid hydrogen storage: a review. Int J Hydrogen Energy 2007;32:1121—40.
[2] George L, Saxena SK. Structural stability of metal hydrides, alanates and borohydrides of alkali and alkali-earth elements: a review. Int J Hydrogen Energy 2011;35:5454—70.
[3] Jain IP, Jain P, Jain A. Novel hydrogen storage materials: a review of lightweight complex hydrides. J Alloys Compd 2010;503:303—39.
[4] Cerón-Hurtado NM, Esquivel MR. Characterization of $LaNi_{4.70}Al_{0.30}$ handled in air and application to a scheme of thermal compression of hydrogen. Int J Hydrogen Energy 2012;37:10376—9.
[5] Obregón SA, Andrade Gamboa JJ, Esquivel MR. Synthesis of Al-containing $MmNi_5$ by mechanical alloying: milling stages, structure parameters and thermal annealing. Int J Hydrogen Energy 2012;37:14972—7.
[6] Ceron-Hurtado NM, Esquivel MR. Stages of mechanical alloying during the synthesis of Sn-containing AB_5-based intermetallics. Int J Hydrogen Energy 2010;35:6057—62.
[7] Langford JL, Delhez R, De Keijser THH, Mittemeijer EJ. Profile analysis for microcrystalline properties by the Fourier and other methods. Aust J Phys 1998;41:173—87.
[8] Obregón SA, Andrade Gamboa JJ, Esquivel MR. On the Al content and characterization of $MmNi_{5-x}Al_x$ synthesized by mechanical alloying. Procedia Mater Sci 2012;1:156—63.
[9] Kisi EH, Buckley CE, Gray EM. The hydrogen activation of $LaNi_5$. J Alloys Compd 1992;185:369—84.
[10] Esquivel MR, Zelaya E, Andrade Gamboa JJ, Obregón SA. Two-fold materials for hydrogen energy applications: synthesis and characterization. Procedia Mater Sci 2012;1:156—63.
[11] Au M, Wang Q. Rare earth-nickel alloy for hydrogen compression. J Alloys Compd 1993;201:115—9.
[12] Kim JK, Park II-S, Kim KJ, Gawlik K. A hydrogen-compression system using porous metal hydride pellets of $LaNi_{5-x}Al_x$. Int J Hydrogen Energy 2008;33:870—7.
[13] Van Mal HH, Buschow KHJ, Miedema AR. Hydrogen absorption in $LaNi_5$ and related compounds: experimental observations and their explanation. J Less Comm Met 1974;35:65—76.
[14] Kim SR, Lee JY. The effect of thermal cycling on the hydriding rate of $MmNi_{4.5}Al_{0.5}$. J Less Comm Met 1990;161:37—47.
[15] Laurencelle F, Dehouche Z, Goyette J, Bose TK. Integrated electrolyser-metal hydride compression system. Int J Hydrogen Energy 2006;31:762—8.
[16] Cieslik J, Kula P, Sato R. Performance of containers with hydrogen storage alloys for hydrogen compression in heat treatment facilities. J Alloys Compd 2011;509:3972—7.
[17] Wan X, Chen R, Zhang Y, Chen C, Wang Q. Hydrogen storage alloys for high-pressure suprapure hydrogen compressor. J Alloys Compd 2006;420:322—5.
[18] Goltsov VA, Veziroglu TN. From hydrogen economy to hydrogen civilization. Int J Hydrogen Energy 2001;26:909—15.
[19] Goltsov VA. Memorandum on the transition from the fossil system to hydrogen economy and then to hydrogen civilization. Int J Hydrogen Energy 2002;27:72—6.